Plasmonics (2020) 15:2033–2042
https://doi.org/10.1007/s11468-020-01216-5

Effect of Size-Dependent Damping on Plasmon-Hybridized Modes of Asymmetric Nanosphere Dimers: the Role of Nanogap, Size Ratio, Surrounding Medium, and Substrate

Sugandh Priya[1] · Venkata Ramanaiah Dantham[1]

Received: 9 March 2020 / Accepted: 21 June 2020 / Published online: 8 July 2020

Abstract
Herein, we report quasi-static theory-based simulations on size-asymmetric Au and Ag nanosphere dimers in which size-dependent damping induced by the electron-surface interaction is prominent. The sensitivity of plasmon-hybridized modes of both asymmetric nanodimers with respect to the size ratio of the nanospheres forming nanodimer, the refractive index of surrounding medium, nanogap, and the local dielectric perturbation in the surrounding medium in the presence of the semi-infinite substrate is studied systematically. In each case, the theoretical sensitivity value is estimated for parallel and perpendicular polarizations. Moreover, for comparison, the dependence of plasmon modes of size-symmetric nanosphere dimers on the size-dependent damping is investigated.

Keywords Plasmon hybridization · Localized surface plasmon resonance · Metal nanoparticles · Nanoplasmonic dimers · Quasi-static theory · Scattering cross section · Substrate effect

Introduction

Recently, plasmonically coupled nanoparticles have gained interest in the field of nanoplasmonics due to their special features such as giant electric field enhancement at the nanometer-sized gaps created between coupled nanoparticles and controllable plasmonic properties. These properties make these coupled nanoparticles fit for various applications like surface-enhanced Raman scattering [1–3], surface-enhanced fluorescence [4], localized surface plasmon resonance sensing [5], plasmon rulers [6], optical tweezers [7], and non-linear optical properties [8, 9]. Nanodimers are basically formed by mutual coupling between plasmons of two interacting nanoparticles separated by a few nanometers. The electric field at the nanogap is always large due to the constructive coupling of the plasmon modes (or overlap of wave functions of electrons of each nanoparticle within the nanogap). Moreover, the far-field plasmonic properties of nanodimer are different from individual nanoparticles due to the variation in their polarizabilities.

✉ Venkata Ramanaiah Dantham
dantham@iitp.ac.in

[1] Department of Physics, Indian Institute of Technology Patna, Bihta, Patna 801103, India

A wide variety of nanodimers such as nanosphere dimers [10–16], nanorod dimers [17], nanocube dimers [18], split nanoring dimers [19], bowtie nanoantenna [20], and mushroom-shaped nanodimers [21] are existing in the literature. However, nanosphere dimers are the most common and widely used for various applications due to relatively simple geometry. Experimentally, nanodimers are synthesized by various methods. Some of them are DNA-assembled [12, 22], electron beam lithography [21], colloidal lithography [23–26], and four-beam holographic lithography [27].

In the case of size-symmetric nanosphere homodimers (for which the size and composition of both nanoparticles are the same), numerical/theoretical simulations have been performed to understand the dependence of the LSPR spectra on (i) interparticle separation [10, 12–15], (ii) dimensions of the nanodimer [12, 15], (iii) dimer composition [10, 11] and (iv) direction of the applied field [13, 16].

Theoretical studies on size-asymmetric nanosphere homodimers (ANSDs) (for which the size of both nanoparticles is different, but the composition of the nanoparticles is the same) are very limited. Experimental and theoretical investigations have been performed to understand the dependence of the optical properties of free-standing Ag ANSDs on the polarization of incident light with the help of discrete dipole approximation (DDA) [16]. Later, Xiang et al. have studied the dependence of plasmon modes of Au ANSDs on the

interparticle separation and size ratio of the nanoparticle-forming nanodimer [12]. It is important to note that the full width at half maximum (FWHM) values of the experimental spectra in both reports were significantly larger than the theoretical spectra. Because the size-dependent damping in nanoparticles originated due to the electron-surface interaction was ignored. Moreover, the dependence of the plasmon modes of Ag ANSDs and Au ANSDs on the surrounding environment and the dielectric substrate has not been explored in the literature. These motivated us to perform theoretical investigation systematically on Au ANSDs and Ag ANSDs by considering damping effects.

Herein, we report (i) the far-field scattering spectra of Ag ANSDs and Au ANSDs with variation of interparticle separation (nanogap size), surrounding medium and size ratio of the nanoparticles for the parallel and perpendicular polarizations, (ii) the effect of size-dependent damping on the scattering spectra of size-symmetric nanosphere homodimers (SNSDs) and ANSDs, and (iii) the role of semi-infinite dielectric substrate on the spectra of Ag ANSDs and Au ANSDs.

Theoretical Aspects

Effective Polarizabilities of Free-Standing Nanosphere Dimers

The value of polarizability of a single nanosphere is independent of the orientation of the nanoparticle with respect to the incident light electric field (***E***) direction due to the three-dimensional symmetry of the nanosphere. However, in case of nanosphere dimer, the value of polarizability becomes sensitive to the direction of ***E***. According to the quasi-static theory, the effective polarizabilities of ANSD are given by [28].

$$\alpha_{\mathrm{ns}}^{\parallel} = \frac{\alpha_{\mathrm{ns1}} + \alpha_{\mathrm{ns2}} + \frac{\alpha_{\mathrm{ns1}}\alpha_{\mathrm{ns2}}}{\pi L^3}}{1 - \frac{\alpha_{\mathrm{ns1}}\alpha_{\mathrm{ns2}}}{\left(2\pi L^3\right)^2}} \tag{1}$$

$$\alpha_{\mathrm{ns}}^{\perp} = \frac{\alpha_{\mathrm{ns1}} + \alpha_{\mathrm{ns2}} - \frac{\alpha_{\mathrm{ns1}}\alpha_{\mathrm{ns2}}}{2\pi L^3}}{1 - \frac{\alpha_{\mathrm{ns1}}\alpha_{\mathrm{ns2}}}{\left(4\pi L^3\right)^2}} \tag{2}$$

Here, $\alpha_{ns}^{\parallel}$ and $\alpha_{ns}^{\perp}$, respectively, are the effective polarizabilities of nanosphere dimer when the ***E*** is parallel and perpendicular to the dimer axis passing through the centers of two nanospheres. L is the center-to-center distance of the spheres in the dimer. α_{ns1} and α_{ns2} are polarizabilities of primitive nanospheres, and these can be expressed as follows

$$\alpha_{\mathrm{ns1,ns2}} = 4\pi R_{1,2}^3 \frac{\varepsilon_{\mathrm{p}} - \varepsilon_{\mathrm{m}}}{\varepsilon_{\mathrm{p}} + 2\varepsilon_{\mathrm{m}}} \tag{3}$$

where R_1 and R_2 are the radii of the primitive nanospheres. ε_{p} and ε_{m} are the electric permittivities of nanosphere and surrounding medium, respectively. The scattering cross sections for free-standing nanosphere dimers for the parallel (||) and perpendicular (⊥) polarizations are given by

$$\sigma_{\mathrm{sca}}^{\parallel,} = \frac{8\pi^3\varepsilon_{\mathrm{m}}^2}{3\lambda^4}\left|\alpha_{\mathrm{ns}}^{\parallel,}(\lambda)\right|^2 \tag{4}$$

The scattering cross section basically represents the amount of power scattered by the nanoparticle over the amount of power per unit area carried by the incident light. It has the dimensions of the area [29]. Here, λ represents the wavelength of incident light. It is to be noted that, for smaller size of nanoparticles (less than bulk mean free path of the metal), the dielectric function becomes size-dependent due to the electron-surface scattering [30, 31] The modified dielectric function of smaller nanoparticles can be written as

$$\varepsilon(\omega) = \varepsilon_{\infty} - \frac{\omega_p^2}{\omega^2 + i\gamma\omega} \tag{5}$$

where,

$$\omega = \frac{c}{\lambda} \tag{6}$$

and

$$\gamma = \gamma_0 + \Delta\gamma \tag{7}$$

$$\Delta\gamma = A_s\frac{v_f}{l} \tag{8}$$

Here ε_{∞}, ω_{p}, γ_0, and c are the dielectric constant at infinite frequency, plasma frequency, bulk damping term, and speed of light respectively. v_{f} and l represent the Fermi velocity and reduced electron mean free path length. For spherical particles, l is simply the diameter [32]. A_{s} is a parameter which depends on the geometry and is equal to 1 for isotropic scattering [32, 33]. In the present work, the values of ε_{∞}, ω_{p}, and γ_0 for Ag nanoparticles are taken as 3.7, 8.9, and 0.021 eV, respectively [30], and for the case of Au, these values are taken as 9.8, 9.0, and 0.072 eV, respectively [34]. The values of v_{f} and c are 1.4×10^6 m/s and 3×10^8 m/s respectively.

Effective Polarizabilities of Substrate-Supported Nanosphere Dimers

It is important to note that the polarizability of any kind of nanoplasmonic particle is a function of depolarization factor. For better clarity, Eq. (3) can be expressed in terms of depolarization factor as follows:

$$\alpha_{\mathrm{ns1,ns2}} = \frac{4\pi R_{1,2}^3(\varepsilon_{\mathrm{P}} - \varepsilon_{\mathrm{m}})}{3[\varepsilon_{\mathrm{m}} + A(\varepsilon_{\mathrm{P}} - \varepsilon_{\mathrm{m}})]} \tag{9}$$

where A is the depolarization factor and it is equal to 1/3 for free-standing spherical nanoparticles irrespective of their dimension and electric permittivity. According to an image-dipole approximation, the polarizabilities of nanospheres placed over a semi-infinite dielectric substrate (shown in Fig. 1) can be written as [35].

$$\alpha^{\mathrm{P},}_{\mathrm{ns1,ns2}} = \frac{4\pi R_{1,2}^3(\varepsilon_{\mathrm{P}}-\varepsilon_{\mathrm{m}})}{3\left[\varepsilon_{\mathrm{m}} + A^{\parallel,\perp}(\varepsilon_{\mathrm{P}}-\varepsilon_{\mathrm{m}})\right]} \tag{10}$$

where

$$A^{\parallel,\perp} = \frac{1}{3}\left[1-\frac{\chi^{\parallel,\perp}}{8}\frac{\varepsilon_{\mathrm{sub}}-\varepsilon_{\mathrm{m}}}{\varepsilon_{\mathrm{sub}}+\varepsilon_{\mathrm{m}}}\right] \tag{11}$$

For dipole moment parallel to the plane, $\chi^{\parallel} = 1$and if it is perpendicular, then$\chi^{\perp} = 2$. ε_{sub} is the electric permittivity of the substrate. It is worthy to mention here that Eq. (10) is independent of the dimensions of the dielectric substrate. However, the role of thickness of the substrate can be included by introducing an additional image dipole, and finally, Eq. (11) can be generalized for finite thickness substrate as [35].

$$A^{\parallel,\perp}_{1,2} = \frac{1}{3}\left[1-\frac{\chi^{\parallel,\perp}}{8}\frac{\varepsilon_{\mathrm{sub}}-\varepsilon_{\mathrm{m}}}{\varepsilon_{\mathrm{sub}}+\varepsilon_{\mathrm{m}}}\right]\left[1-f\left(t_{\mathrm{sub}},R_{1,2}\right)\right] \tag{12}$$

Where $f\,(t_{sub},\ R_{1,2})$ is the thickness dependent factor given by

$$f\left(t_{\mathrm{sub}},R_{1,2}\right) = \frac{4\varepsilon_{\mathrm{sub}}\varepsilon_{\mathrm{m}}}{\left(\varepsilon_{\mathrm{sub}}+\varepsilon_{\mathrm{m}}\right)^2}\left[\frac{1}{1+\left(t_{\mathrm{sub}}/R_{1,2}\right)}\right]^3 \tag{13}$$

Here, $t_{\mathrm{sub}}/R_{1,2} >> 1$. After substituting Eqs. (12) and (13) in Eq. (10), one can get the polarizabilities of substrate-supported individual nanospheres of different radii. If we substitute these polarizabilities in Eqs. (1) and (2), then the effective polarizabilities of substrate-supported ANSD for parallel and perpendicular polarizations would be obtained. It is important to note that the ε_{p} needs to be replaced by $\varepsilon(\omega)$ in Eqs. (9) and (10) for obtaining the effective polarizabilities of smaller nanoparticles placed on a dielectric substrate. The formation of different plasmon-hybridized modes of ANSDs for parallel and perpendicular polarizations of the incident light and the effect of size-dependent damping on the hybridized modes are shown schematically in Fig. 2.

Results and Discussion

As mentioned above, the present manuscript emphasizes on studying the effect of size-dependent damping on plasmon-hybridized modes of ANSDs. It is well-known that the size-dependent damping effects become prominent for the smaller size of the nanoparticles, where the quasi-static regime is valid. Due to this, we have taken a radius of the individual nanosphere not more than 20 nm for our calculations. To study the effect of distance (D) on the scattering spectra, the D values are varied from 1 to 40 nm. Beyond 40 nm, the plasmon-plasmon coupling is found to be extremely weak, and below 1 nm, the classical or electrodynamical models are insufficient to describe the dimer response, and quantum tunneling is expected to come into the picture [36].

Effect of *D* on the Plasmon-Hybridized Modes

Panels (a) and (b) of Fig. 3, respectively, show the far-field scattering spectra (plots of far-field scattering cross section vs. wavelength) of Ag ANSD with the variation of interparticle separation when the size-dependent damping effect has been taken into consideration for parallel and perpendicular polarizations respectively. These spectra are obtained using Eqs. (1), (2), (3), (4), (5), (6), (7), and (8). From this figure, we can conclude that in case of Ag ANSD, two peaks have been observed for both parallel and perpendicular polarizations which represent bonding and anti-bonding modes. The plasmon-plasmon coupling in the nanosphere dimer can be viewed as molecular hybridization [13, 16]. In the case of parallel polarization, the lower energy modes and higher

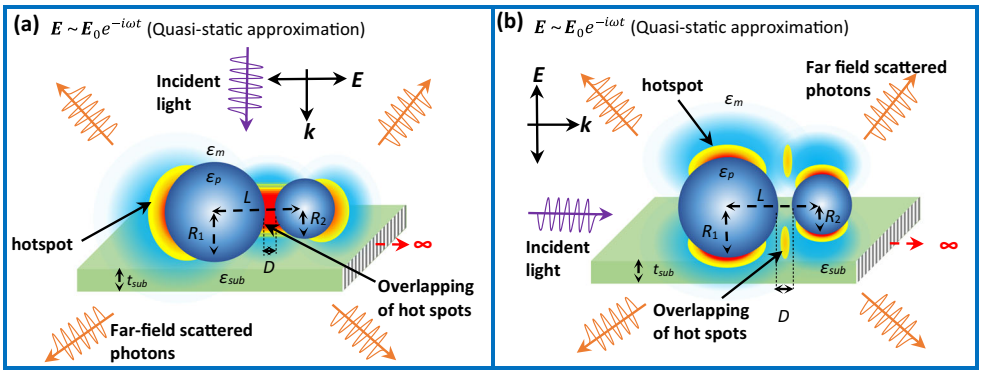

Fig. 1 Panels (**a**) and (**b**) show the illustration of substrate-supported ANSD excited with the light polarized parallel and perpendicular to the dimer axis, respectively. Here, E_0 is the amplitude of electric field and ω is the angular frequency of light. D is the interparticle separation, and t_{sub} is the thickness of the dielectric substrate

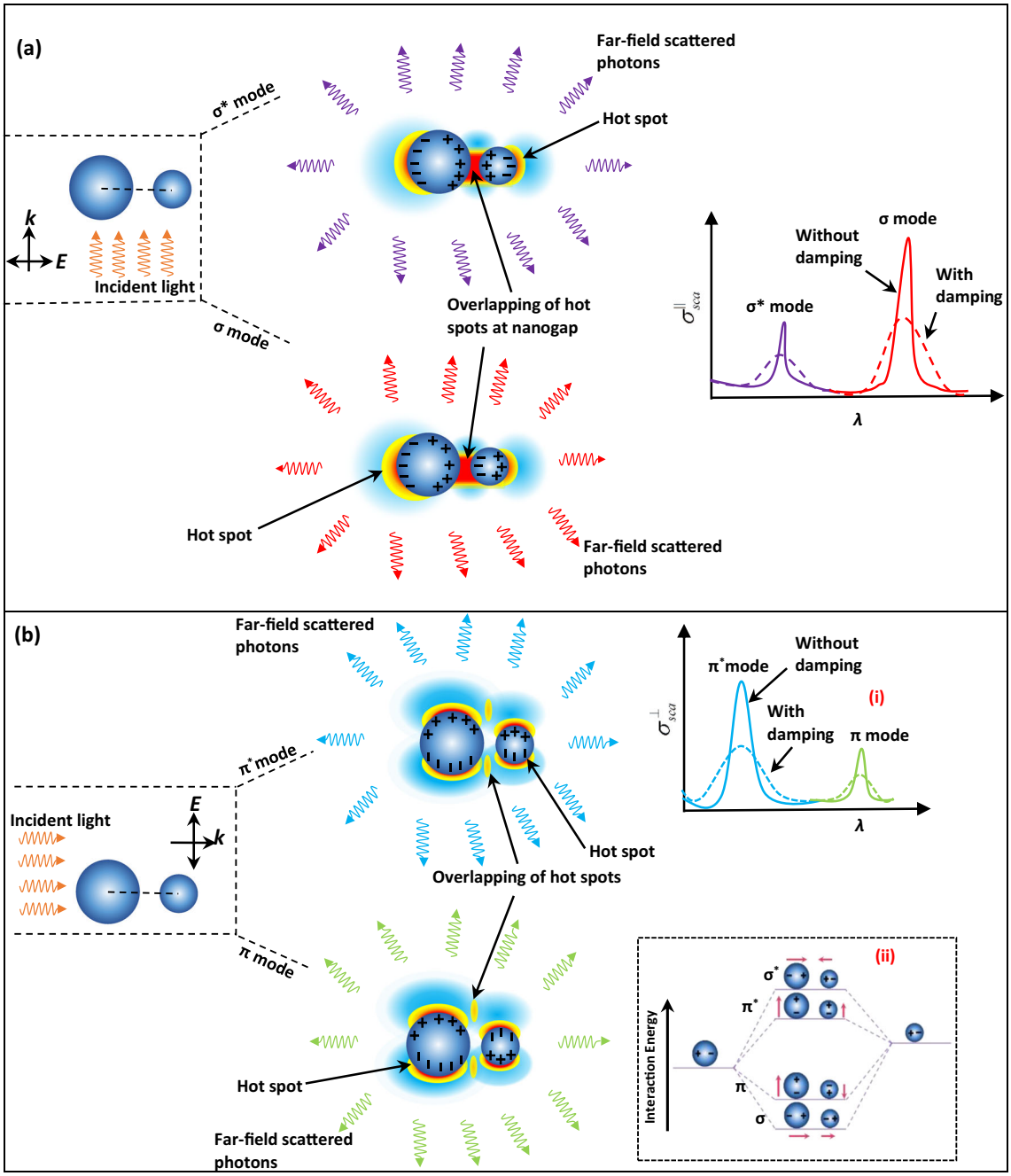

Fig. 2 Panel (**a**) shows the formation of two different plasmon-hyrbridized modes (anti-bonding (σ^*) and bonding (σ) modes) and scattering of light by ANSD when the $\boldsymbol{E}$ is parallel to the dimer axis (parallel polarization). The effect of size-dependent damping on the σ and σ^* modes observed in the scattering spectrum is also shown schematically here. Panel (**b**) shows the formation of two different plasmon-hyrbridized modes (anti-bonding (π^*) and bonding (π) modes) and scattering of light by ANSD when the $\boldsymbol{E}$ is perpendicular to the dimer axis (perpendicular polarization). The effect of size-dependent damping on the π and π^* modes is shown in inset (i). Inset (ii) shows the schematic diagram of energy levels of plasmon-hybridized modes of the ANSD

energy modes are commonly known as σ and σ^* modes, and for the perpendicular polarization, these modes are called as π and π^* (shown in Fig. 2).

Panels (c) and (d) show the scattering spectra of Ag ANSD, when the size-dependent damping effects have been ignored. These spectra are obtained using Eqs. (1) to (7) by keeping $\Delta\gamma = 0$. From panels (a)–(d), it is apparent that the plasmon modes are broadened significantly in the presence of the size-dependent damping effects. However, the change in FWHM of the plasmon modes in case of parallel and perpendicular polarizations is nearly same. In addition, the wavelength locations of the modes are found nearly the same in the presence and absence of the size-dependent damping. Panel (e) shows the variation of the wavelength separation

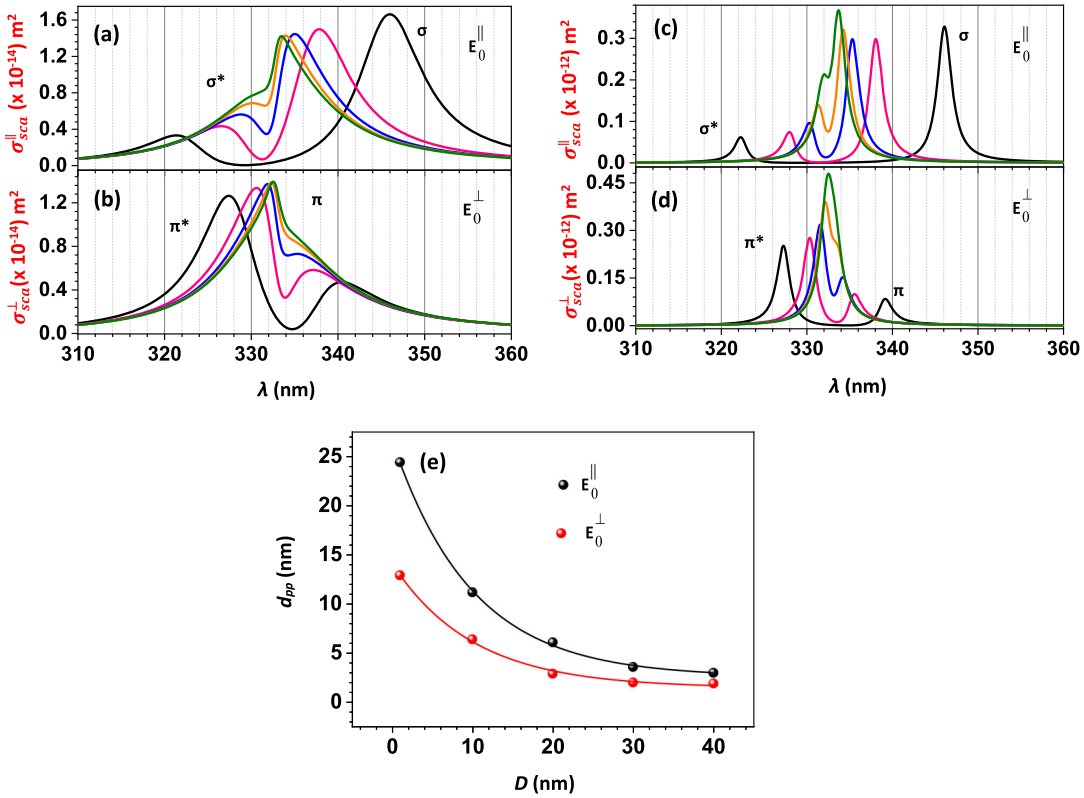

Fig. 3 Panels (**a**) and (**b**) show the polarization dependence of plasmon modes of Ag ANSD ($R_1 = 20$ nm and $R_2 = 6$ nm) with the consideration of the size-dependent damping effect. Panels (**c**) and (**d**) show the plasmon modes of the same nanodimer without considering size-dependent damping effect. In Panels (**a**)–(**d**), black (−), pink (-), blue (-), orange (-), and olive green (-) curves, respectively, represent the spectra obtained for $D = 1$ nm, 10 nm, 20 nm, 30 nm, and 40 nm. Panel (**e**) shows the variation of d_{pp} value with D

between the plasmon modes (d_{pp}) with D, and it is found to decrease exponentially upon increasing D due to the weakening of the plasmon-plasmon coupling with the increase of D. For a fixed D, the wavelength separation between the π and π^* modes is found lower as compared with the separation between the σ and σ^* modes because of relatively weaker plasmon-plasmon coupling in case of perpendicular polarization.

Table 1 shows the change in the FWHM ($\Delta\lambda$) values of plasmon modes of ANSD observed at different D values. From this table, it is apparent that (i) the FWHM values of the plasmon modes are found to increase nearly 4 times than those observed in the absence of the damping effects, and (ii) the role of D is insignificant on the FWHM values. In order to check whether the damping effects are prominent in SNSDs or ANSDs, theoretical investigation has also been carried out on SNSD, and the FWHM values of plasmon modes are listed in Table 1. From the table, it is apparent that the FWHM values are much larger in case of SNSD in the presence of the damping effects as compared with those observed in case of ANSD. In addition, these values are found to increase further significantly upon decreasing the size of the SNSD due to the predominant damping effects.

Table 1 Estimation of change in $\Delta\lambda$ values of plasmon modes of Ag ANSDs and Ag SNSDs observed for parallel polarization. Here, $\Delta\lambda_w$ and $\Delta\lambda_{w/o}$ are FWHM values of plasmon modes with and without size-dependent damping effects, respectively. In case of ANSD, calculations have been done only for σ mode

S. No.	λ_{mode} (nm)	D (nm)	$\Delta\lambda_w$ (nm)	$\Delta\lambda_{w/o}$ (nm)	$\Delta\lambda_w/\Delta\lambda_{w/o}$
ANSD; $R_1 = 20$, $R_2 = 6$ nm					
1	346	1	7.9	2.0	3.9
2	338	10	7.6	1.9	4.0
3	335	20	6.8	1.9	3.6
4	334	30	6.6	1.9	3.5
SNSD; $R_1 = R_2 = 20$ nm					
1	358	1	17.0	2.1	8.1
2	345	10	15.9	2.0	7.9
3	340	20	15.4	2.0	7.7
4	337	30	15.1	1.9	7.9
SNSD; $R_1 = R_2 = 6$ nm					
1	354	1	49.6	2.4	20.6
2	337	10	45.4	1.9	23.9
3	335	20	44.1	1.9	23.2
4	334	30	43.6	1.8	24.2

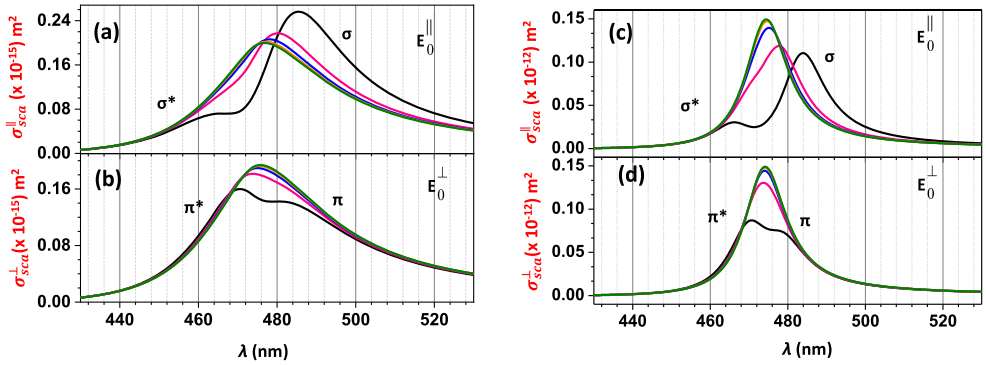

Fig. 4 Panels (**a**) and (**b**) show the polarization dependence of plasmon modes of Au ANSD ($R_1 = 20$ nm and $R_2 = 6$ nm) with the consideration of size-dependent damping effect. Panels (**c**) and (**d**) show the plasmon modes of the same ANSD without considering the size-dependent damping effects. In all these panels, black (−), pink (-), blue (-), orange (-), and olive green (-) curves, respectively, represent the modes obtained for $D = 1$ nm, 10 nm, 20 nm, 30 nm, and 40 nm

Figure 4 shows the scattering spectra of Au ANSD in the presence and absence of the size-dependent damping effects. From panels (a)–(d) of Fig. 4, it is easy to conclude that the FWHM values of the plasmon modes are reasonably broadened in the presence of damping as in the case of Ag ANSDs. However, the change in the FWHM values in the presence of size-dependent damping is more in the case of Ag ANSDs as compared with the Au ANSDs. For example, the FWHM of the σ mode in the case of Ag nanodimer is increased by around 4 times in the presence of the damping when $D =$ 1 nm, whereas in case of Au nanodimers, it is increased only by nearly 2 times. It is also worth to mention here that even though the value of d_{pp} is nearly same, there is a significant overlap between σ and σ^* and π and π^* modes in the case of Au nanodimers due to larger FWHM of the plasmon modes as compared with the Ag nanodimers. Larger broadening of the plasmon modes in Au is due to larger imaginary part of the refractive index of the Au as compared with Ag.

Effect of ε_m on the Plasmon-Hybridized Modes

In order to understand the effect of surrounding medium on plasmon modes, the far-field scattering spectra of Ag ANSD are obtained by varying the ε_m and considering size-dependent damping effects. Panel (**a**) of Fig. 5 shows the far-field scattering spectra obtained after varying ε_m from 1.00 to 2.62 for the case of parallel polarization. From this figure, it is apparent that the σ and σ^* modes are found to shift

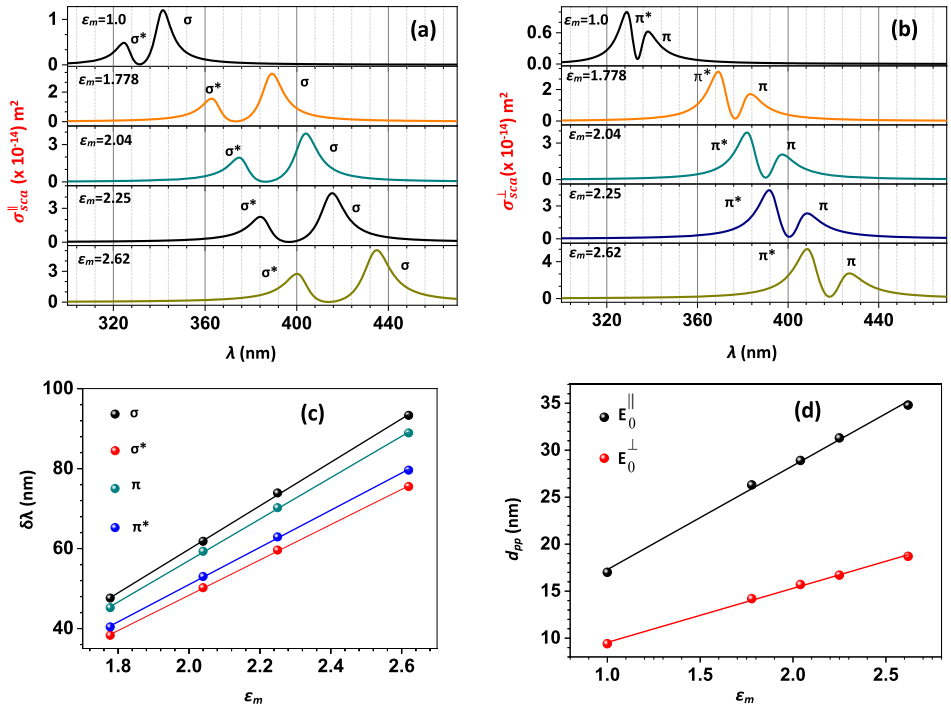

Fig. 5 Panels (**a**) and (**b**) show the effect of ε_m on plasmon modes of Ag ANSD with $R_1 =$ 20 nm and $R_2 = 4$ nm for parallel and perpendicular polarizations, respectively. The variation in $\delta\lambda$ values of different plasmon modes with ε_m is shown in panel (**c**). Panel (**d**) shows the variation of d_{pp} with ε_m for different polarizations

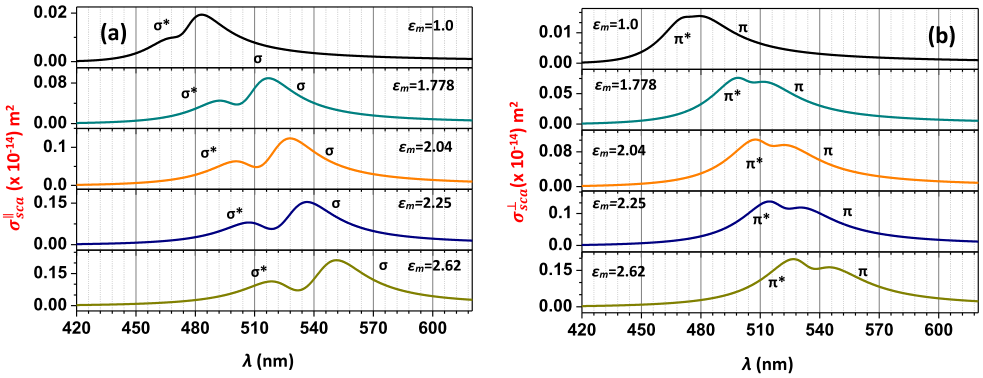

Fig. 6 Panels (**a**) and (**b**) show the effect of ε_m on plasmon modes of Au ANSD with R_1 = 20 nm and R_2 = 4 nm for parallel and perpendicular polarizations, respectively

to higher wavelengths with the increase of ε_m. In addition, the FWHM and intensity of the modes are found to increase slightly with value of ε_m. Panel (b) shows the far-field spectra obtained for different ε_m for the case of perpendicular polarization. In this case also, π and π^* modes are red-shifted with the increase of ε_m. From panel (c), it is clear that the shift in wavelength ($\delta\lambda$) of σ, σ^*, π, and π^* modes is found to increase linearly with the ε_m.

Among all modes, σ mode is found to have better refractive index sensitivity. d_{pp} in case of parallel polarization is found about 2 times larger as compared with perpendicular polarization (panel (d)). For comparison, theoretical investigation has been carried out for Au ANSD by varying the ε_m for the case of parallel and perpendicular polarizations and obtained scattering spectra are shown in Fig. 6. From this figure, it is apparent that all the observed modes are red-shifted, and the d_{pp} value is increased upon increasing the value of ε_m as in the case of Ag ANSD. However, $\delta\lambda$ values of the plasmon modes observed in the case of Ag ANSD are 1.5 times larger as compared with those observed in the case of Au nanodimer.

Effect of Size Ratio of the Nanospheres (R_1/R_2) on Plasmon-Hybridized Modes

Panel (a) of Fig. 7, shows the variation in the scattering spectra of Ag ANSD for different R_1/R_2 values when the applied field is parallel to the dimer axis. It is apparent that the d_{pp} value increases on decreasing the value of R_1/R_2. In other words, the magnitude of the blue and red shifts of the σ^* and σ modes is found to increase on decreasing the value of R_1/R_2, respectively.

Similarly, the π and π^* mode separation is also observed to increase on decreasing the value of R_1/R_2 (panel (b)). However, for a fixed R_1/R_2 value, the magnitude of d_{pp} is more for the case of parallel polarization. To understand the dependence of the d_{pp} with respect to R_1/R_2 value, a plot

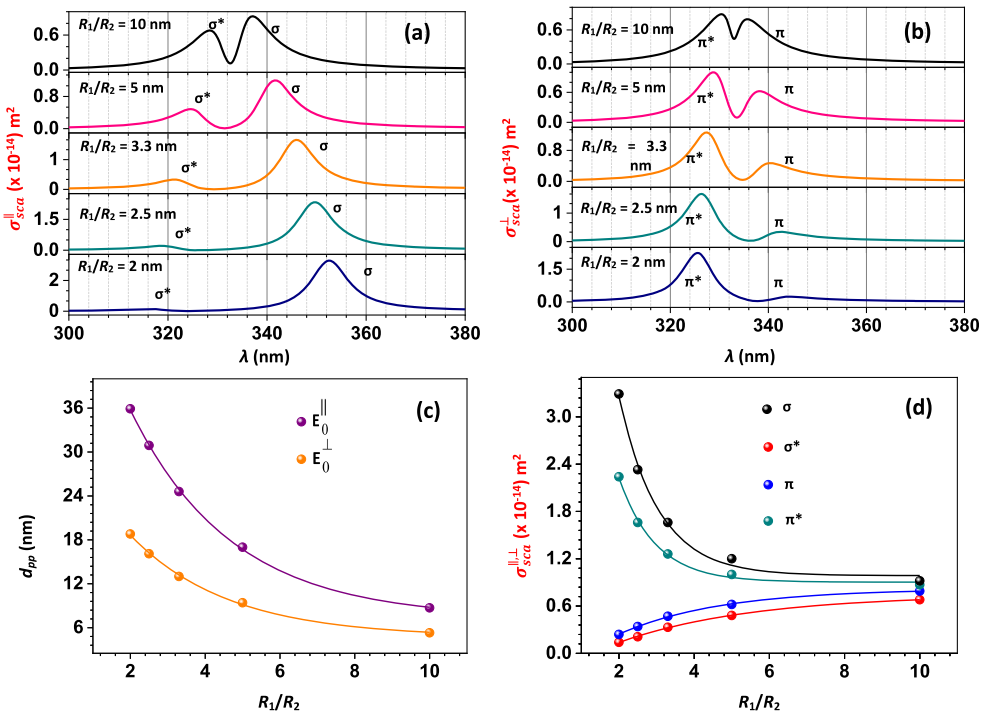

Fig. 7 Panels (**a**) and (**b**) show the effect of R_1/R_2 on plasmon modes of Ag ANSD for parallel and perpendicular polarizations, respectively. Panels (**c**) and (**d**), respectively, show the effect of R_1/R_2 on the d_{pp} and maximum value of σ_{sca} at plasmon mode wavelength

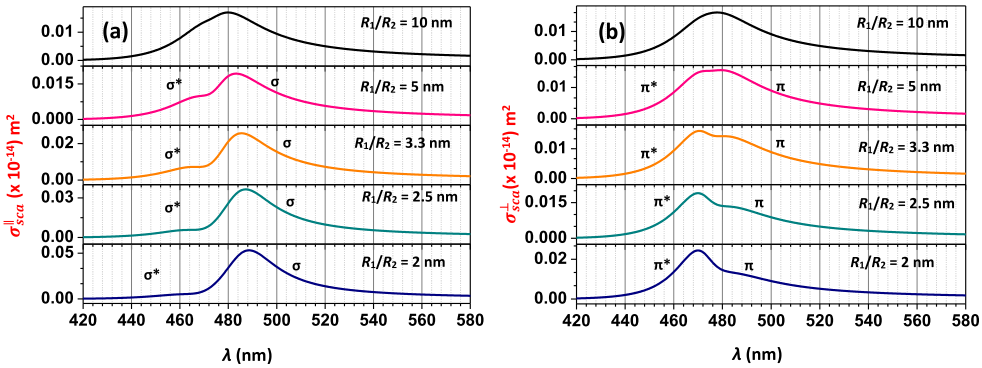

Fig. 8 Panels (**a**) and (**b**) show the effect of R_1/R_2 on plasmon modes of Au ANSD for parallel and perpendicular polarizations, respectively

between d_{pp} and R_1/R_2 is made and shown in panel (c). From this plot, it is clear that the d_{pp} decreases exponentially with R_1/R_2 value. The variation in the intensity of the σ, σ*, π, and π* modes with R_1/R_2 is shown separately in panel (d) for better clarity. It is clear that the intensity of the σ* and π modes is found to increase with R_1/R_2 due to the increase of mismatch in the number of oppositely oriented dipoles on the two nanoparticles. It is worthy to mention here that in case of SNSD, these two modes disappear due to cancellation of the equal but oppositely oriented dipoles on two nanoparticles. In contrast, the amplitude of the σ and π* modes is found to decrease rapidly with the increase of R_1/R_2 values. Figure 8 shows the variation in far-field scattering spectra of Au ANSD with R_1/R_2 values. For the same R_1/R_2 value, the d_{pp} value is significantly smaller as compared with that obtained in Ag ANSD. Moreover, the $\delta\lambda$ value is appreciably lower in Au ANSD.

Effect of ε_{sub} on Plasmon-Hybridized Modes

To understand the effect of dielectric substrate on σ, σ*, π, and π* modes of Ag ANSD, theoretical simulations have been carried out on Ag ANSD placed on different semi-infinite dielectric substrates (shown in panels (a) and (b) of Fig. 9). The scattering spectra of substrate-supported nanodimers have been obtained using Eqs. (4), (10), (11), (12), and (13). From this figure, it is apparent that all plasmon modes are red-shifted upon increasing the value of ε_{sub}. The intensity of the

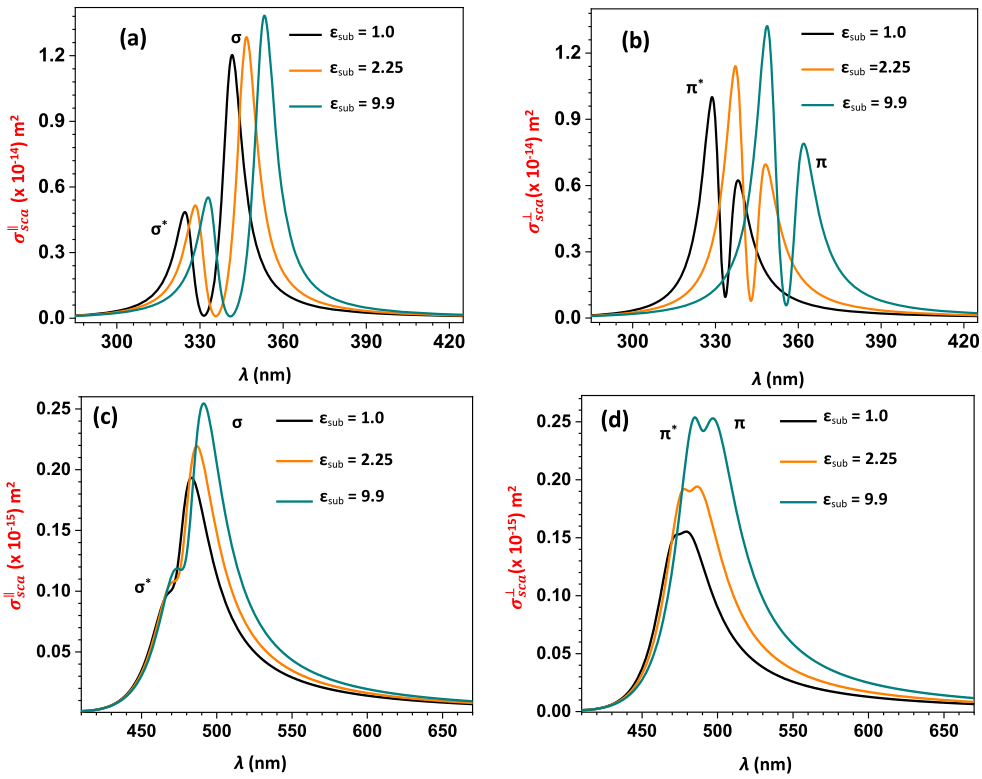

Fig. 9 Panels (**a**) and (**b**) show the effect of ε_{sub} on plasmon modes of Ag ANSD for parallel and perpendicular polarizations, respectively. Panels (**c**) and (**d**) show the effect of ε_{sub} on plasmon modes of Au ANSD for parallel and perpendicular polarizations, respectively

Table 2 Estimation of substrate induced wavelength shifts of the plasmon modes of Ag ANSD ($R_1 = 20$ nm; $R_2 = 4$ nm, $D = 1$ nm) for parallel and perpendicular polarizations. λ_σ, λ_{σ^*}, λ_π, and λ_{π^*} are the wavelengths of σ, σ^*, π, and π^* modes, respectively. $(\delta\lambda_\sigma)_{sub}$, $(\delta\lambda_{\sigma^*})_{sub}$, $(\delta\lambda_\pi)_{sub}$, and $(\delta\lambda_{\pi^*})_{sub}$ are the wavelength shifts of σ, σ^*, π, and π^* modes in the presence of the substrate, respectively

S. No.	Nanoparticle type	ε_{sub}	λ_σ (nm)	λ_{σ^*} (nm)	$(\delta\lambda_\sigma)_{sub}$ (nm)	$(\delta\lambda_{\sigma^*})_{sub}$ (nm)
Parallel polarization						
1	ANSD without substrate	-	341.6	324.6	-	-
2	ANSD with substrate ($t_{sub} = 100$ nm)	2.25	346.7	328.3	5.1	3.7
		9.9	353.3	332.9	11.7	8.3
Perpendicular polarization						
1	ANSD without substrate	-	338.2	328.8	-	-
2	ANSD with substrate ($t_{sub} = 100$ nm)	2.25	348.2	337.2	10.0	8.4
		9.9	361.2	348.7	23.0	19.9

modes has been found to increase slightly with increase in value of ε_{sub}, whereas d_{pp} value is not affected significantly on increasing the value of ε_{sub}. However, d_{pp} is found to increase significantly upon increasing the value of ε_m (Fig. 5). This clearly indicates that the strength of the dielectric perturbation in the surrounding medium due to the variation of ε_m value is larger than that originated due to the variation of ε_{sub} value. Table 2 shows the obtained substrate induced shifts $(\delta\lambda)_{sub}$ of σ, σ^*, π, and π^* modes as a function of ε_{sub} and direction of the applied electric field. From this table, it is clear that the plasmon modes observed in the case of perpendicular polarization are found more sensitive relative to the modes observed for the case of parallel polarization. This is possible due to more overlapping of the local field of the dimer with the dielectric substrate in the case of perpendicular polarization.

Theoretical simulations have also been carried out on Au ANSD placed on different dielectric substrates. The variation in the scattering spectra with the value of ε_{sub} is shown in panels (c) and (d) of Fig. 9. From this figure, it is apparent that for the same ε_{sub}, the $(\delta\lambda)_{sub}$ and d_{pp} values are fairly lower as compared with the case of Ag ANSD. In order to understand the role of D on $(\delta\lambda)_{sub}$, the scattering spectra were obtained by varying the D values from 1 to 40 nm for Ag and Au ANSDs, and observed that the effect of D on $(\delta\lambda)_{sub}$ is insignificant.

Conclusions

Using quasi-static approach, theoretical investigation has been carried out systematically on free-standing and substrate-supported Ag and Au ANSDs, in which the size-dependent damping is prominent. In both types of ANSDs, the plasmon-hybridized modes are observed for parallel and perpendicular polarizations. The increment in the FWHM values of plasmon modes due to the size-dependent damping is more in Ag ANSDs as compared with Au ANSDs. The damping effects are to found to affect the FWHM values of the plasmon modes more in the SNSDs as compared with ANSDs. The bonding modes are blue-shifted, and the anti-bonding modes are red-shifted upon increasing the D value. The value of d_{pp} is found to decrease exponentially on increasing the value of D. For a fixed value of D, the value of d_{pp} is found large in case of parallel polarization. Interestingly, the wavelengths of the observed modes as well as the value of d_{pp} are found to increase with the refractive index of the surrounding medium. The values of d_{pp}, wavelength, and intensity of the plasmon modes are extremely sensitive to the size ratio of the nanospheres (R_1/R_2).

The bonding modes are relatively more sensitive to the dielectric perturbation introduced by the dielectric substrate. The obtained $(\delta\lambda)_{sub}$ values are nearly independent of D. The value of $(\delta\lambda)_{sub}$ of plasmon modes is observed larger in the case of perpendicular polarization. Even though the wavelengths of the plasmon modes are red-shifted with the increase of ε_{sub}, the d_{pp} value found nearly remains unaffected unlike in the case of the change in ε_m. As compared with plasmon-hybridized modes of Au ANSDs, the modes of Ag ANSDs are relatively more sensitive with respect to ε_m, ε_{sub}, and R_1/R_2. To the best of our knowledge, all the observations mentioned above would be useful for optimizing performance of the plasmonic devices based on free-standing and substrate-supported asymmetric metal nanosphere dimers.

Funding Information The authors received funding from the Council of Scientific and Industrial Research (CSIR), Government of India, under Grant 03(1406)/17/EMR-II.

References

1. Nam JM, Oh JW, Lee H, Suh YD (2016) Plasmonic nanogap-enhanced Raman scattering with nanoparticles. Acc Chem Res 49:2746–2755
2. Yue W, Wang Z, Whittaker J, Lopez-royo F, Yang Y, Zayats AV (2017) Amplification of surface-enhanced Raman scattering due to

substrate-mediated localized surface plasmons in gold nanodimers. J Mater Chem C 5:4075–4084
3. Hoflich K, Becker M, Leuchs G, Christiansen S (2012) Plasmonic dimer antennas for surface enhanced Raman scattering. Nanotechnology 23:185303
4. Park JE, Kim J, Nam JM (2017) Emerging plasmonic nanostructures for controlling and enhancing photoluminescence. Chem Sci 8:4696–4704
5. Zhang S, Xu H (2016) Tunable dark plasmons in a metallic nanocube dimer: toward ultimate sensitivity nanoplasmonic sensors. Nanoscale 8:13722–13729
6. Visser EWA, Horacek M, Zijlstra P (2018) Plasmon rulers as a probe for real-time microsecond conformational dynamics of single molecules. Nano Lett 18:7927–7934
7. Juan ML, Righini M, Quidant R (2011) Plasmon nano-optical tweezers. Nat Photonics 5:349–356
8. Butet J, Bernasconi GD, Martin OJF (2018) Silencing the second harmonic generation from plasmonic nanodimers: a comprehensive discussion. Beilstein J Nanotechnol 9:2674–2683
9. Panoiu NC, Sha WEI, Lei DY, Li GC (2018) Nonlinear optics in plasmonic nanostructures. J Opt 20:083001
10. Roopak S, Pathak NK, Sharma R, Ji A, Pathak H, Sharma RP (2016) Numerical simulation of extinction spectra of plasmonically coupled nanospheres using discrete dipole approximation: influence of compositional asymmetry. Plasmonics 11:1603–1612
11. Sharma R, Pathak NK, Sharma RP (2018) Computational study of plasmon interaction in organic media: a comparison between analytical and numerical model for dimer. Plasmonics 13:1775–1784
12. Lan X, Chen Z, Liu B, Ren B, Henzie J, Wang Q (2013) DNA-directed gold nanodimers with tunable sizes and interparticle distances and their surface plasmonic properties. Small 9:2308–2315
13. Chen F, Alemu N, Johnston RL (2011) Collective plasmon modes in a compositionally asymmetric nanoparticle dimer. AIP Adv 1: 032134
14. Marhaba S, Bachelier G, Bonnet C, Broyer M, Cottancin E, Grillet N, Lerme J, Vialle J, Pellarin M (2009) Surface plasmon resonance of single gold nanodimers near the conductive contact limit. J Phys Chem C 113:4349–4356
15. Khlebtsov B, Melnikov A, Zharov V, Khlebtsov N (2006) Absorption and scattering of light by a dimer of metal nanospheres: comparison of dipole and multipole approaches. Nanotechnology 17:1437–1445
16. Sheikholeslami S, Jun Y, Jain PK, Alivisatos AP (2010) Coupling of optical resonances in a compositionally asymmetric plasmonic nanoparticle dimer. Nano Lett 10:2655–2660
17. Muskens OL, Giannini V, Sanchez-Gil JA, Rivas JG (2007) Optical scattering resonances of single and coupled dimer plasmonic nanoantennas. Opt Express 15:17736–17746
18. Knebl D, Horl A, Trugler A, Kern J, Krenn JR, Puschnig P, Hohenester U (2016) Gap plasmonics of silver nanocube dimers. Phys Rev B 93:081405
19. Khan AD, Khan SD, Khan R, Ahmad N, Ali A, Khalil A, Khan FA (2014) Generation of multiple Fano resonances in plasmonic split nanoring dimer. Plasmonics 9:1091–1102
20. Kaniber M, Schram K, Regler A, Bartl J, Glashagen G, Flassig F, Wierzbowski J, Finley JJ (2016) Surface plasmon resonance spectroscopy of single bowtie nano-antennas using a differential reflectivity method. Sci Rep 6:23203
21. Xiang Q, Li Z, Zheng M, Liu Q, Chen Y, Yang L, Jiang T, Duan H (2018) Sensitive SERS detection at the single particle level based on nanometer-separated mushroom-shaped plasmonic dimers. Nanotechnology 29:105301
22. Paulo PMR, Botequim D, Joskowiak A, Martins S, Prazeres DMF, Zijlstra P, Costa SMB (2018) Enhanced fluorescence of a dye on DNA-assembled gold nanodimers discriminated by lifetime correlation spectroscopy. J Phys Chem C 122:10971–10980
23. Fang L, Liu D, Wang Y, Li Y, Song L, Gong M, Li Y, Deng Z (2018) Nanosecond-laser-based charge transfer plasmon engineering of solution-assembled nanodimers. Nano Lett 18:7014–7020
24. Hakonen A, Svedendahl M, Ogier R, Yang ZJ, Lodewijks K, Verre R, Shegai T, Andersson PO, Kall M (2015) Dimer-on-mirror SERS substrates with attogram sensitivity fabricated by colloidal lithography. Nanoscale 7:9405–9410
25. Shegai T, Chen S, Miljkovic VD, Zengin G, Johansson P, Kall M (2011) A bimetallic nanoantenna for directional colour routing. Nat Commun 2:481
26. Shegai T, Johansson P, Langhammer C, Kall M (2012) Directional scattering and hydrogen sensing by bimetallic Pd−Au nanoantennas. Nano Lett 12:2464–2469
27. Luo Y, Li X, Zhang X, Prybolsky S, Shepard GD, Strauf S (2016) Tunable multipole resonances in plasmonic crystals made by four-beam holographic lithography. Appl Phys Lett 108:053105
28. Lombardi A, Grzelczak MP, Crut A, Maioli P, Pastoriza-Santos I, Liz-Marzan LM, Fatti ND, Vallee F (2013) Optical response of individual Au-Ag@SiO2 heterodimers. ACS Nano 7:2522–2531
29. Frezza F, Mangini F, Tedeschi N (2018) Introduction to electromagnetic scattering: tutorial. J Opt Soc Am A 35:163–173
30. Foreman MR, Vollmer F (2013) Theory of resonance shifts of whispering gallery modes by arbitrary plasmonic nanoparticles. New J Phys 15:083006
31. Schelm S, Smith GB (2005) Evaluation of the limits of resonance tunability in metallic nanoshells with a spectral averaging method. J Opt Soc Am A 22:1288
32. Nehl CL, Grady NK, Goodrich GP, Tam F, Halas NJ, Hafner JH (2004) Scattering spectra of single gold nanoshells. Nano Lett 4: 2355–2359
33. Averitt RD, Sarkar D, Halas NJ (1997) Plasmon resonance shifts of Au-coated Au_2S nanoshells: insight into multicomponent nanoparticle growth. Phys Rev Lett 78:4217
34. Derkachova A, Kolwas K, Demchenko I (2016) Dielectric function for gold in plasmonics applications: size dependence of plasmon resonance frequencies and damping rates for nanospheres. Plasmonics 11:941–951
35. Kadkhodazadeh S, Christensen T, Beleggia M, Mortensen NA, Wagner JB (2017) The substrate effect in electron energy-loss spectroscopy of localized surface plasmons in gold and silver nanoparticles. ACS Photonics 251:261
36. Scholl JA, Etxarri AG, Koh AL, Dionne JA (2013) Observation of quantum tunneling between two plasmonic nanoparticles. Nano Lett 13:564–569